

High-Efficiency Resonant Beam Charging and Communication

Yunfeng Bai, Qingwen Liu, *Senior Member, IEEE*, Xin Wang, *Fellow, IEEE*,
Yudan Gou, Bin Zhou and Zhiyong Bu

Abstract—With the development of Internet of Things (IoT), demands of power and data for IoT devices increase drastically. In order to resolve the supply-demand contradiction, simultaneous wireless information and power transfer (SWIPT) has been envisioned as an enabling technology by providing high-power energy transfer and high-rate data delivering concurrently. In this paper, we introduce a high-efficiency resonant beam (RB) charging and communication scheme. The scheme utilizes the semiconductor materials as gain medium, which has a better energy absorption capacity compared with the traditional solid-state one. Moreover, to match the gain size and reduce the transmission loss, the telescope internal modulator (TIM) are adopted in the scheme, which can concentrate beams. To evaluate the scheme SWIPT performance, we establish an analytical model and study the influence factors of its beam transmission, energy conversion, output power, and spectral efficiency. Numerical results shows that the proposed RB system can realize 16 W electric power output with 11 % end-to-end conversion efficiency, and support 18 bit/s/Hz spectral efficiency for communication.

Index Terms—Optical communication; Resonant beam communications; Wireless power transfer; Wireless charging

I. INTRODUCTION

Accompany by the growth of the Internet of Things (IoT), network capacity continues to increase due to rapidly growing number of devices [1]. At the same time, the energy consumption of mobile devices is also increasing dramatically to support high-performance communication and computation [2]. Facing these challenges, various technologies have been promoted, e.g., wireless power transfer (WPT), ultra-dense cloud radio access networks, etc. [3], [4]. Among them, WPT for providing unlimited energy supply is undoubtedly one of the most attractive solutions [5]. Compared with wired power supply, WPT is flexible and suitable for mobile devices; compared with battery, WPT is not restricted by battery's capacity, weight, or volume [6], [7].

Based on the WPT, simultaneous wireless information and power transfer (SWIPT) technology has attracted great attention by researchers to address both the energy and data

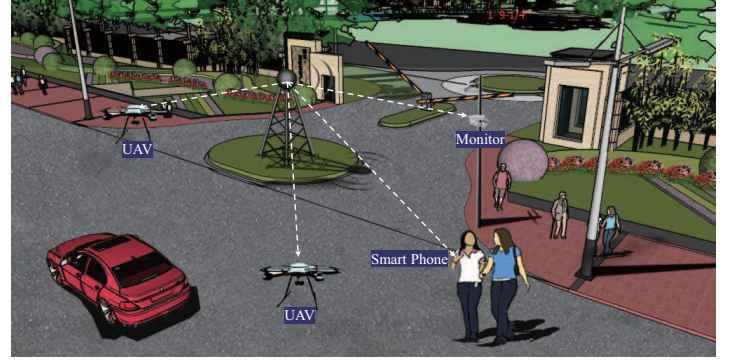


Fig. 1. Application scenarios of SWIPT (UAV: unmanned aerial vehicle)

demands at the same time (Fig. 1). SWIPT technologies have many forms with different system structure depending on the carrier. SWIPT system utilizing radio frequency (RF) as carrier is one of typical schemes. It depends on the mature RF communication technology, which has low cost, long transfer distance, and expansive coverage. However, in the presence of high density RF radiation, humans may be physical damage. Therefore, the researchers must gain more thorough understanding of potential health and safety impacts associated with the usage of SWIPT in public settings [8]. Optical beams such as visible light can also be the SWIPT carrier. This scheme could support high power energy transfer, and has the great communication potential of huge license free spectrum, no electromagnetic interference, and high data rates [9], [10]. However, typical Optical beams schemes are limited by alignment, coverage area, etc.

As one of the optical beams scheme, resonant beam system (RBS) was proposed for high-power, self-alignment, and human safety wireless energy transfer [11], [12]. The transmitter of the RBS is combined with the receiver to form a spatially separated resonator (SSR). The resonant beam generates in the cavity and carrying energy and information transfers between the transmitter and the receiver through the reflectors. Due to the beam concentration characteristics, RBS can support high power transfer [13]. Moreover, by cooperating retro-reflectors, RBS enables self-alignment between the transmitter and the receiver for mobile SWIPT [14]. When the light path between the transmitter and the receiver is blocked thanks to the separate resonant cavity structure, the cyclic reciprocating process of the resonant beam in the cavity will interrupt immediately, which prevents foreign objects from continuous

Y. Bai, and Q. Liu, are with the College of Electronics and Information Engineering, Tongji University, Shanghai, China, (email: baiyf@tongji.edu.cn, qliu@tongji.edu.cn).

Xin Wang is with the Key Laboratory for Information Science of Electromagnetic Waves, Department of Communication Science and Engineering, Fudan University, Shanghai 200433, China (e-mail: xwang11@fudan.edu.cn).

Yudan Gou is with the College of Electronics and Information Engineering, Sichuan University, Chengdu 610065, China(gouyudan@scu.edu.cn).

B. Zhou, and Z. Bu, are with the Key Laboratory of Wireless Sensor Network and Communications, Shanghai Institute of Microsystem and Information Technology, Chinese Academy of Sciences, Shanghai, China, (email: bin.zhou@mail.sim.ac.cn, zhiyong.bu@mail.sim.ac.cn).

radiative exposure, ensuring the human safety [15].

Besides, as the aforementioned statement, since the light beam is the signal carrier in the RBS, it can allow high-rate data transfer [16].

Due to these remarkable advantages, the RBS has been applied in various SWIPT applications such as unmanned aerial vehicles (UAV), smartphones, laptops, etc. [17], [18]. The theoretical model, system design, deployment of the RBS have been studied in the literature recently. In addition to the theoretical analysis, Zhang *et al.* verified that the RBS can support 2 W WPT with 1 % end-to-end conversion efficiency in experiment [13]. Sheng *et al.* demonstrated an efficient, long-distance scheme using cat-eye reflectors to realize transmitter alignment, a telescope to concentrate beams, and adopting aspheric lenses to fix spherical aberration [19]. In [20], Zhang *et al.* characterized a long vertical external-cavity surface-emitting lasers resonator scheme for wireless charging. Moreover, to support multi-devices access into the RBS, Xiong *et al.* proposed a time-division multiple access (TDMA) RBS design for wireless power transfer [21]. Xiong *et al.* proposed the RB communication design and the analytical model in [22]. Liu *et al.* presented the basic SWIPT model of the RBS and demonstrated its mobile ability using the retro-reflectors [14]. To evaluate the safety of the RBS, Fang *et al.* proposed an analytical model based on electromagnetic field analysis and assessed its safety with external object invasion [15].

Previous research has underscored the potential of Resonant Beam (RB) technology in Simultaneous Wireless Information and Power Transfer (SWIPT). Nevertheless, the original RB scheme have been challenged by significant energy conversion losses, resulting in a merely approximate 1% energy conversion efficiency across short distances [13]. The relatively low conversion efficiency of this technology presents challenges for its application in power supply scenarios for devices under a low-carbon and energy-saving context. Moreover, due to the suboptimal transmission efficiency, the system requires a greater input to satisfy the power demand at the output end. This situation imposes further challenges on system cooling, safety, and component durability.

In this study, we present a novel RB-SWIPT scheme designed to elevate both power transmission efficiency and communication efficacy. We propose the use of a semiconductor gain medium, in contrast to the conventional solid-state medium. Semiconductors exhibit superior energy absorption capacity from the pump source, thus promoting a more effective energy level transition and population inversion efficiency. Consequently, the power threshold decreases, thereby improving the overall conversion efficiency.

Additionally, we integrate a Telescope Internal Modulator (TIM) into the resonator. The TIM serves to compress the beam, thereby harmonizing with the smaller dimensions of the gain medium and subsequently reducing transmission loss. This strategic modification underlines our commitment to enhancing the efficiency of SWIPT systems.

The contributions of this paper are summarized as follows:

- A high-efficiency RB-SWIPT scheme is proposed. By adopting the semiconductor gain medium and the tele-

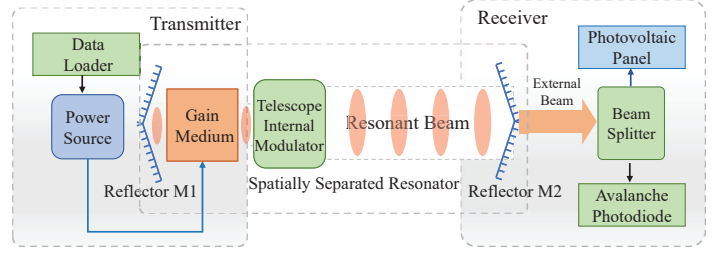


Fig. 2. High-efficiency resonant beam SWIPT system

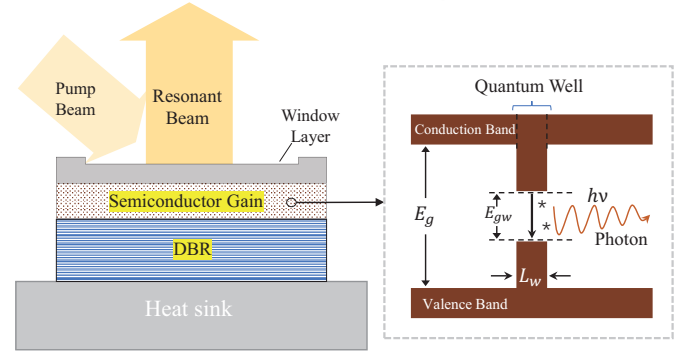


Fig. 3. Transmitter structure and operating principles of the semiconductor gain (DBR: distributed Bragg reflector; E_g , E_{gw} : energy level difference; L_w : quantum well length; $h\nu$: photon energy)

scope internal module (TIM), the scheme can achieve high-power, high-rate, and conversion efficiency enhanced SWIPT.

- An analytical model of the scheme is presented, which describes the energy conversion, the beam propagation, the electric power output, and data transfer capability. A feasible evaluation method for system performance and a guidance for parameters optimization is provided.

The rest of the paper is organized as follows. In Section II, the model of the high-efficiency RBS involving the semiconductor gain medium and TIM is described. In section III, the numerical evaluation of the system performance is depicted. The concerns on beam splitting process is discussed in Section IV. In section V, the conclusion is presented.

II. SCHEME ANALYSIS AND MODEL ESTABLISHMENT

In this section, we will state the function principle of the scheme on realizing high-efficiency resonant beam charging and communication and develop the analytical model.

A. System Structure and Semiconductor Gain

The system structure is briefly depicted in Fig. 2. Overall, the system can be divided into three parts: transmitter, receiver, and spatially separated resonator. The transmitter is mainly composed of a gain medium, a pump source and a data loader. The data loader can load the electric signal into the pump source for data transfer. Then, the pump source releases beam carrying the data signal in the form of optical radiation to the gain medium. The gain medium receives the energy and occurs

the stimulated absorption, spontaneous emission, and stimulated emission, generating photons to form resonant beams. The receiver mainly includes three elements: photovoltaic (PV) panel module, beam splitter, and avalanche photodiode (APD) module [23], [24]. The beam splitter accepts the external beams output from the M2 and splits them into two rays for energy harvesting and data receiving. The PV module can convert beam energy into electrical power for charging. The APD module is used to detect the data signal. The spatially separated resonator is made by reflectors M1, M2, and a TIM. Among them, M1 and M2 constitute the resonant cavity for beams oscillation. Subject to material properties, the size of the gain medium is usually relatively small in order to achieve high conversion efficiency. Thus, the beam size is usually greater than the gain medium, which causes unignorable beam loss. The TIM is placed on the optical path in front of the gain, which is used to change the phase of the resonant beam for beam compression and promoting the beam incidence.

The proposed RB scheme applies the semiconductor materials to compose the gain medium for efficiency enhanced. Semiconductor material utilizes the recombination of electrons in the conduction band and holes in the valence band to generate simulated radiation [25], which has the following characteristics: 1) The materials with different ingredients on gain medium developing window layer, active area, and distributed Bragg reflector layer (DBR) have a band-gap difference forming a potential barrier. It will confine electrons and holes within the gain area, which is conducive to the recombination of electrons and holes; 2) The active area and the cladding layers have a refractive index difference. When photons transfer on the material boundary, they will be reflected back to the active area. As a result, the light field can be restricted in the active area, which causes more stimulated radiation generation; 3) The semiconductor gain can be made as a hetero-junction quantum well structure. This structure (Fig. 3) can further reduce the thickness of the active layer to the nano-level producing the quantum effect, which makes the limitation of carriers and light fields be further strengthened, and causes the energy level difference decreasing from E_g to E_{gw} [26], [27]. Overall, thanks to these characteristics, the loss of the particle conversion in semiconductor gain can be quite small, and the threshold value will be greatly reduced.

B. Resonant Beam Power and Conversion Efficiency

In the proposed system, photons generated on the semiconductor gain medium propagate within the cavity, forming the resonant beam. Then, resonant beams carry the energy and signal arrive at the receiver. We can use the beam power output on the reflector M2 as the figure of merit to evaluate the transmission performance.

Due to the presence of energy loss, there is a threshold power in the system; the beam output is only available when the input power is greater than the threshold condition. In addition, there is a conversion efficiency ratio between the input and output power of the system, which is determined by the process of energy conversion at each stage. Based on

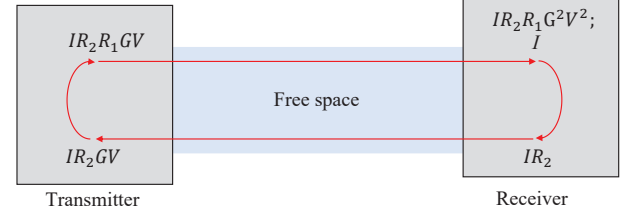


Fig. 4. End-to-end energy cycle (I : initial energy density; R_1, R_2 : reflectivity of M1, M2; G : gain factor; V : Path loss)

the cyclic power principle and materials characteristic of the gain [28], [29], the external beam power can be defined as:

$$P_{\text{beam}} = (P_{\text{in}} - P_{\text{th}}) \eta_s, \quad (1)$$

where P_{in} denotes the input electric power, P_{th} expresses the threshold power, and η_s is the slope efficiency.

Firstly, η_s is related to the system structure such as the reflectivity of M1, which can be expressed as:

$$\eta_s = \frac{\eta_{pc} \eta_{pa} \lambda_{\text{pump}} \ln(R_2)}{\lambda_{\text{beam}} \ln(R_1 R_2 V)}, \quad (2)$$

where R_1 and R_2 denote the reflectivity of the reflectors M1 and M2, η_{pc} is the pump conversion efficiency, λ_{beam} , λ_{pump} represent the wavelength of resonant beams and pump beams, $V = V_c V_d$ expresses overall energy losses mainly including constant loss V_c (absorption dispersion of reflectors and air, internal loss in the gain), and beam diffraction loss V_d .

Then, P_{th} determines by the gain medium, which can be depicted as:

$$P_{\text{th}} = \frac{A_s h c l N_{\text{th}}}{\lambda \eta_{pc} \eta_{pa} \tau}, \quad (3)$$

where A_s expresses the effective active cross-section, h denotes the Planck constant, c is the speed of light in vacuum, λ represents the beam wavelength, l is the length of the gain medium, N_{th} denotes the threshold carrier density in gain medium, η_{pa} expresses the pump absorption efficiency, τ is the carrier attenuation time. τ is determined by N_{th} , which can be expressed as [29]:

$$\tau = (\alpha + \beta N_{\text{th}} + \gamma N_{\text{th}}^2)^{-1}, \quad (4)$$

where α , β and γ express materials' recombination coefficients. N_{th} is related to the gain factor of gain medium, which can be described as:

$$N_{\text{th}} = N_0 \exp(g/g_0), \quad (5)$$

where g_0 is gain coefficient under low pump power, N_0 denotes the transparency carrier density, and g expresses the saturation gain coefficient.

To define g , we need to analyze the energy saturation condition where the gain and loss are in a balance [28]. According to Fig. 2, the cavity includes reflectors M1, M2, TIM, and gain medium. Resonant beams propagate in the cavity and passes through these components. In this process, optical elements such as M1 will absorb or reflect part of beam causing energy loss. In contrast, energy gains on the gain medium. Thus, after one round-trip, if the beam returns to

the origin point and its energy is unchanged, we can conclude that the system achieves the balance of loss and gain. This equilibrium condition is called a saturation condition which is depicted in Fig. 4. As can be seen, after one-trip energy cycle, the initial energy density will become $IR_2R_1G^2V^2$ from I . When the saturation condition is satisfied, the $IR_2R_1G^2V^2$ should equal to I , and parameters have the relationship as:

$$R_1R_2G^2V^2 = 1, \quad (6)$$

where $G = \exp(\Gamma gl)$ express the overall gain factor. Each time the beam travels through the gain, the beam energy intensity will increase by G times. R_1 and R_2 can be considered as the beam emission ratio of M1 and M2. Then, g can be defined as:

$$g = -\frac{\ln(R_1R_2V^2)}{2l}. \quad (7)$$

Further, taking the (7) into (5), the N_{th} can be expressed as:

$$N_{th} = N_0(R_1R_2V^2)^{-(2g_0l\Gamma)^{-1}}, \quad (8)$$

where Γ denotes the longitudinal confinement factor.

Finally, based on aforementioned formulas, the formula of P_{beam} presented in (1) can be depicted. Furthermore, the beam transmission efficiency can be defined as:

$$\eta_b = \frac{\eta_{pc}\eta_{pa}\lambda_{pump}\ln(R_2)}{\lambda_{beam}\ln(R_1R_2V)} \left(1 - \frac{A_s h c l N_{th}}{\lambda \eta_{pc} \eta_{pa} \tau P_{in}}\right). \quad (9)$$

C. Beam Transmission Description and Diffraction Loss

To analyze the resonator structure, the process of beam transmission in the resonator should be described at first. In this paper, we adopt beam vectors and transmission matrices to define the beam propagation. Specifically, based on the beam characteristics (straight line propagating), we can depict it as $\vec{r} = (x, \theta_x)$, where x expresses the position parameter on the coordinate axis and θ_x represents the propagation direction of the beam. Then, we assume that a beam at the origin is transmitting in free space, from x_1 to x_2 , and its direction angle of transmission is θ_1 . Using the beam vector, it can be expressed as $\vec{r}_1 = (x_1, \theta_1)$. Then, after the beam travels to z position along the light path, the beam vector becomes $\vec{r}_2 = (x_2, \theta_2)$. The process of vectors conversion from \vec{r}_1 to \vec{r}_2 can utilize matrix \mathbf{M} to express, which is $\vec{r}_2 = \mathbf{M}\vec{r}_1$. Moreover, when the beam passes through a series of optical components, the entire process can be expressed as the matrices of these components multiplied in the corresponding order.

Utilizing transmission matrices, we can define the optical elements and beam transfer in the cavity. Firstly, we adopt it to depict reflectors. The reflectors introduce in the scheme involving in a lens and a reflective mirror. The lens is a convex lens whose focal length is f . The reflective mirror is located at the exit pupil of the lens with distance d , and its surface is flat.

The lenses and mirror usually can use typical matrices [28] to express. Thus, the reflector can be described as:

$$\mathbf{M}_r = \begin{bmatrix} 1 & f \\ 0 & 1 \end{bmatrix} \begin{bmatrix} 1 & 0 \\ -1/f & 1 \end{bmatrix} \begin{bmatrix} 1 & d \\ 0 & 1 \end{bmatrix} \begin{bmatrix} 1 & 0 \\ 0 & 1 \end{bmatrix} \begin{bmatrix} 1 & d \\ 0 & 1 \end{bmatrix} \begin{bmatrix} 1 & 0 \\ -1/f & 1 \end{bmatrix} \begin{bmatrix} 1 & f \\ 0 & 1 \end{bmatrix} \quad (10)$$

$$= \begin{bmatrix} -1 & 0 \\ 1/f_r & -1 \end{bmatrix},$$

where

$$f_r = \frac{f^2}{2(d-f)}. \quad (11)$$

To realize ideal retro-reflect, we can take $d = f$, which denotes the mirror is put at the focal point of the lens. Reflectors can reflect incident beams back toward the parallel path of the original one, which is precondition of the self-alignment [14].

Then, we apply the matrix to express the TIM. The TIM is introduced to compress resonant beams. In Fig. 5, lenses L1, L2 with focal length f_1 , f_2 compose the TIM, which can be depicted as:

$$\mathbf{M}_{TIM} = \mathbf{M}_{L_2} \mathbf{M}_1 \mathbf{M}_{L_1}$$

$$= \begin{bmatrix} 1 & 0 \\ -\frac{1}{f_2} & 1 \end{bmatrix} \begin{bmatrix} 1 & l_t \\ 0 & 1 \end{bmatrix} \begin{bmatrix} 1 & 0 \\ -\frac{1}{f_1} & 1 \end{bmatrix} \quad (12)$$

$$= \begin{bmatrix} \frac{1}{M} & l_t \\ 0 & M \end{bmatrix},$$

where $M = -f_1/f_2$. From (12), the beam Assuming a beam with vector $\vec{r}_1 = (x_1, 0)$ enters the TIM, according to (12), it will become $\vec{r}_2 = (x_1/M, 0)$ after being modulated by the TIM. From a macro perspective, the beam is toward to light axes with ratio M . If $M > 1$, it denotes that the beam is compressed.

Finally, based on the above matrices and Fig. 5, we can define the one trip beams transmission in the resonator. Taking reflector M1 as the starting point, the beam propagating in the cavity will pass through lens 1, lens 2, and reflector M2 in sequence. Using matrices to express those process which is:

$$\mathbf{M}_c = \mathbf{M}_{M_2} \mathbf{M}_{d_3} \mathbf{M}_{L_2} \mathbf{M}_1 \mathbf{M}_{L_1} \mathbf{M}_{d_2} \mathbf{M}_{d_1} \mathbf{M}_{M_1}$$

$$= \begin{bmatrix} -1 & 0 \\ \frac{1}{f_{r2}} & -1 \end{bmatrix} \begin{bmatrix} 1 & d_3 \\ 0 & 1 \end{bmatrix} \begin{bmatrix} 1 & 0 \\ -\frac{1}{f_2} & 1 \end{bmatrix} \begin{bmatrix} 1 & l_t \\ 0 & 1 \end{bmatrix} \begin{bmatrix} 1 & 0 \\ -\frac{1}{f_1} & 1 \end{bmatrix} \begin{bmatrix} 1 & d_2 \\ 0 & 1 \end{bmatrix} \begin{bmatrix} 1 & d_1 \\ 0 & 1 \end{bmatrix} \begin{bmatrix} -1 & 0 \\ \frac{1}{f_{r1}} & -1 \end{bmatrix}, \quad (13)$$

where \mathbf{M}_{M_1} , \mathbf{M}_{M_2} , \mathbf{M}_{L_1} , and \mathbf{M}_{L_2} express the matrix of reflector M1, M2 with effective curvature factors ρ_1 and f_{r2} , and lenses L1, L2 with focal length f_1 and f_2 . \mathbf{M}_{d_1} , \mathbf{M}_{d_2} , \mathbf{M}_{d_3} , and \mathbf{M}_1 express the beam transfer in the space with distances d_1 , d_2 , d_3 and l_t .

Beam spot is the distribution of the beam in the vertical propagation direction, and its radius is usually used to evaluate the lateral amplitude of the beam at a certain point. According to [30], [31], the beam spots radius on the reflectors of the resonant cavity can be defined by \mathbf{M}_c . Besides, since the gain medium is designed to be located on the transmitter, and d_1 is small. It can be considered that the spot size on the gain is

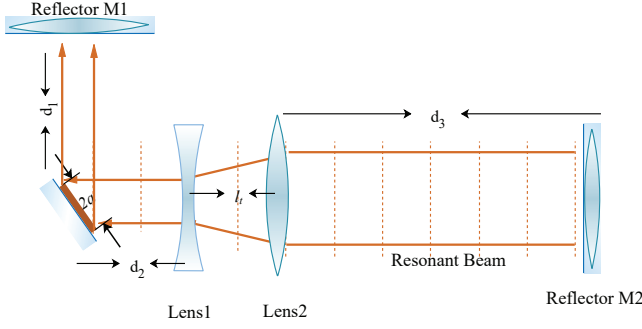


Fig. 5. Resonator structure (d_1, d_2, d_3, l_t : elements distance; a : radius of gain medium)

approximately equal to the spot size on M1. In this case, the beam spot radius on the gain medium can be given by:

$$\begin{cases} \mathbf{M}_c = \begin{bmatrix} A_c & B_c \\ C_c & D_c \end{bmatrix} \\ \omega_g = \left(-\frac{\lambda^2 B_c D_c}{\pi^2 A_c C_c} \right)^{1/4}, \end{cases} \quad (14)$$

where A_c , B_c , C_c , and D_c are the matrix elements of \mathbf{M}_c which is depicted in (13); λ is the wavelength of the resonant beam. Then, we can utilize ω_g to evaluate the performance of beam compression by TIM. Further, the beam diffraction loss V_d can be also defined as [32]:

$$V_d = 1 - \exp(-2a^2/w_g^2), \quad (15)$$

where a denotes radius of gain medium.

D. Electric Power output and Spectral Efficiency

According to Section II.A, the external beam with signal will output from the reflector M2 at the receiver. Then, the beam splitter can divide the external beam into two. One part will be transferred to the PV cell for electric energy harvesting (EH). The other part will be caught by the APD for data receiving.

1) *Electric power output*: Firstly, part of the external beam separated by the beam splitter is transmitted to the surface of the photovoltaic cell through a homogenizing waveguide. Then, the beam will be converted into electrical power output through photoelectric conversion. This process can be briefly expressed by the following formula [33]:

$$\begin{cases} P_p = \mu P_{\text{beam}}, \\ P_{\text{Eout}} = \eta_p P_p + P_{\text{pth}}, \end{cases} \quad (16)$$

where μ is the power split ratio, P_p expresses the beam power received by the PV. The parameter η_p is the slope efficiency of photoelectric conversion, and P_{pth} is the threshold power of PV. It is worth noting that, to simplify the simulation process, according to the experimental results of [34], P_{Eout} is expressed by a linear model, where the PV is under ideal heat dissipation and receiving area conditions. In practice, the beam energy absorbed by PV is limited, it is expected that the conventional linear EH model is only accurate for the specific

scenario when the received powers at the receiver is in a constant power range and the nonlinear EH model has a better applicability [35]. Further, the end-to-end energy conversion efficiency is depicted as:

$$\eta_E = \frac{\eta_p P_p + P_{\text{pth}}}{P_{\text{in}}}. \quad (17)$$

2) *Spectral efficiency*: The remaining part of the external beam separated by the beam splitter will act on the APD. The APD converts the optical signal into an electrical signal while receiving the data. This process can be depicted as:

$$\begin{cases} P_D = (1 - \mu) P_{\text{beam}}, \\ I_{\text{Dout}} = \nu P_D, \end{cases} \quad (18)$$

where ν is the optical-to-electrical conversion responsivity of APD.

When APD is receiving data, photoelectric conversion will produce thermal noise and shot noise. Among them, thermal noise can be expressed by the following formula [36]:

$$n_{\text{thermal}}^2 = \frac{4kTB_x}{R_L}, \quad (19)$$

where k is the Boltzmann constant, T is the background temperature, and R_L is the load resistor. Moreover, the formula about the shot noise factor is [36]

$$n_{\text{shot}}^2 = 2q(I_{\text{Dout}} + I_{\text{bg}})B_x, \quad (20)$$

where q is the electron charge, B_x is the bandwidth, I_{bg} is the background current. At this point, the additive white Gaussian noise (AWGN) of the communication module can be defined:

$$N_M^2 = n_{\text{shot}}^2 + n_{\text{thermal}}^2. \quad (21)$$

Finally, we can obtain spectral efficiency of the system as [37]:

$$\tilde{C} = \frac{1}{2} \log_2 \left(1 + \frac{I_{\text{Dout}}^2}{2\pi e N_M^2} \right), \quad (22)$$

where e is the natural constant.

III. SIMULATION CALCULATIONS AND RESULTS ANALYSIS

In this section, we will evaluate the performance of the proposed system by analyzing the resonant beam distribution, received beam power, output electric power and channel capacity.

A. Resonant Beam Distribution

In order to match the semiconductor gain, the proposed RB system introduce a built-in TIM, which can modulate the phase of the beam to achieve the beam compression. To evaluate the compression performance, we focus on the beam spot, analyzing its changes with different structure parameters. Since the intensity cross-section of the beam is circular, we adopt the spot radius to evaluate it.

1) *Parameter Setting*: The gain medium is composed of semiconductor material GaAsP, which can generates resonant beam with 980 nm wavelength. It is placed obliquely and is 20 mm away from M1 (d_1). Based on to Section II.C, we set the value of f_{r1} as infinite ($d = f$). Then, to constrain

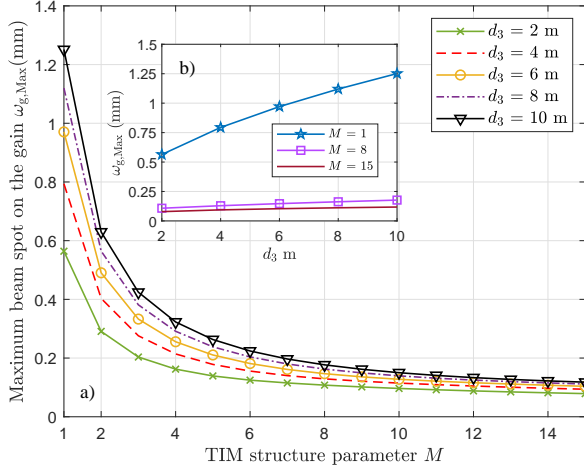


Fig. 6. a) Maximum beam radius on the gain versus TIM structure parameter for different curvature of reflector M2; b) Maximum beam radius on the gain versus end-to-end distance

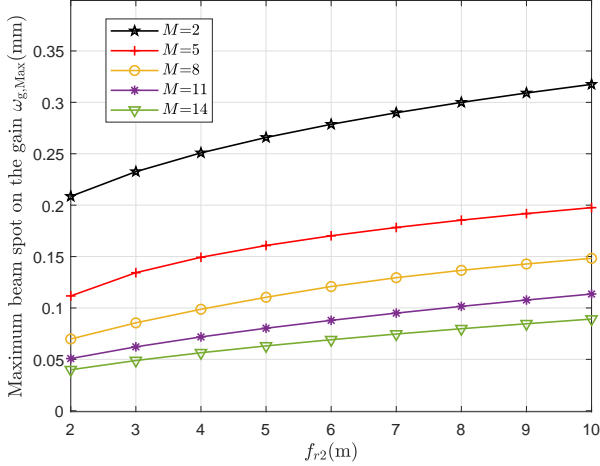


Fig. 7. Maximum beam radius on the gain versus f_r parameters of reflector M2 with different TIM structure parameter

the beam to maintain par-axial propagation, the f_{r2} of M2 is set as variable. The TIM is positioned on the side of the gain medium, and its position parameter is set to $d_2 = 20$ mm relative to the gain chip. The focal length of the concave lens of the TIM is designed as $f_1 = -5$ mm. We set end-to-end distances d_3 from 2 m to 10 m, and TIM structure parameter M as the inspection point, respectively. Moreover, considering the beam spot radius will be different at different distances, we take the maximum value of the spot radius $\omega_{g,Max}$ on the gain medium to evaluate.

2) *Calculation results and analysis*: Fig. 6(a) depicts the relationship of the TIM structure parameter M and the maximum beam spot radius $\omega_{g,Max}$. As can be seen, when the value of M increases, the $\omega_{g,Max}$ shows a downward trend. When M is in the range of 2 to 6, the beam radius decreases rapidly. Then, when M is greater than 10, the decline of the beam spot tends to be gentle, which indicates that compression capacity is limited, if the M is beyond the range, the compression tends

TABLE I
PARAMETERS OF THE GAIN MEDIUM [29]

Parameter	Symbol	Value
Gain factor	g_0	2000 cm^{-1}
Transparency carrier density	N_0	$1.7 \times 10^{18} \text{ cm}^{-3}$
Longitudinal confinement factor	Γ	2.0
Light speed	c	$3 \times 10^8 \text{ m/s}$
Planck constant	h	$6.6260693 \times 10^{-34} \text{ J}\cdot\text{s}$
Monomolecular recombination coefficient	α	10^7 sec^{-1}
Bimolecular recombination coefficient	β	$10^{-10} \text{ cm}^3/\text{sec}$
Auger recombination coefficient	γ	$6 \times 10^{-30} \text{ cm}^6/\text{sec}$

to be stable. Moreover, if d_3 takes a large value, the overall $\omega_{g,Max}$ will increase. In numerical, the beam radius can be compressed from 1.2 mm ($M=1$) to around 0.1 mm, which is only 1/12 of the original beam. Fig. 6(b) presents curves of $\omega_{g,Max}$ as a function of d_3 . As it depicted, in the original scheme without TIM ($M=1$), the radius of beam presents a great trend of increase when d_3 enhances. In contrast, the proposed scheme with TIM shows a gentle trend of increase. Numerically, the value of $\omega_{g,Max}$ in proposed scheme is below 0.25 mm while the original scheme is great then 0.5 mm. Further, we analyze the influence of f_r parameter on beam compression. Fig. 7 shows curves of maximum beam radius on the gain versus f_r parameters of reflector M2. As is shown from the curves, $\omega_{g,Max}$ presents an upward trend with the increase of f_{r2} . Then, curves move down as the value of M increases. Overall, the increase of f_{r2} brings a negative effect on beam compression, as the beam spot enlarging.

Based on the aforementioned analysis, preliminary conclusions can be obtained that the TIM can effectively compress the beam under different end-to-end distance. Based on Section II.A&B, this ability ensures that the resonant beam can enter the micron-level size semiconductor gain without causing large energy loss (V_d).

B. Received Beam Power

According to Section II.A, after the energy accumulating, the external beam will eventually emerge from reflector M2. Then, it will enter the PV and APD respectively under the function of the beam splitter, realizing the electric power output and data reception. Thus, we can adopt the received beam power P_{beam} to evaluate the end-to-end beam transmission performance.

1) *Parameter Setting*: The gain medium is made of GaAsP. According to the material properties, we set the characteristic parameters such as light quantum, gain factor, etc. and listed them in Table I. Furthermore, the pump source adopts a commercial high-efficiency laser diode whose electro-optical conversion efficiency η_{pc} and absorption efficiency η_{pa} are 0.6 and 0.85, the effective active cross-section A_s set as $3 \times 10^{-4} \text{ cm}^2$, constant loss V_c takes 0.99, geometric radius of gain medium a is 0.5 mm, the pump beam wavelength is 808 nm, reflectivity of mirror in M1 is 0.999, and the end-to-end transmission distance is 10 m.

2) *Calculation results and analysis*: Firstly, Fig. 8 describes the relationship of the received beam power, conversion efficiency, and thickness of the effective gain layer. As can be

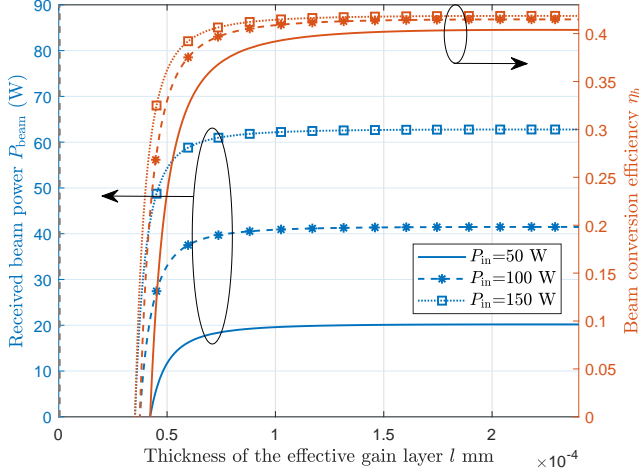


Fig. 8. Received beam power and conversion efficiency versus thickness of the effective gain layer

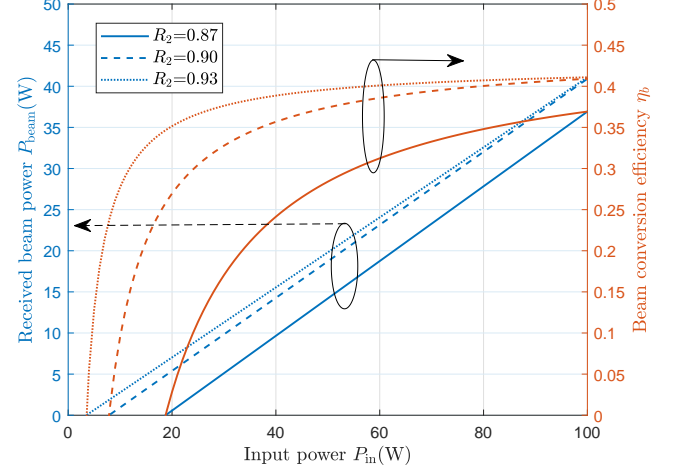


Fig. 10. Received beam power and conversion efficiency versus input power

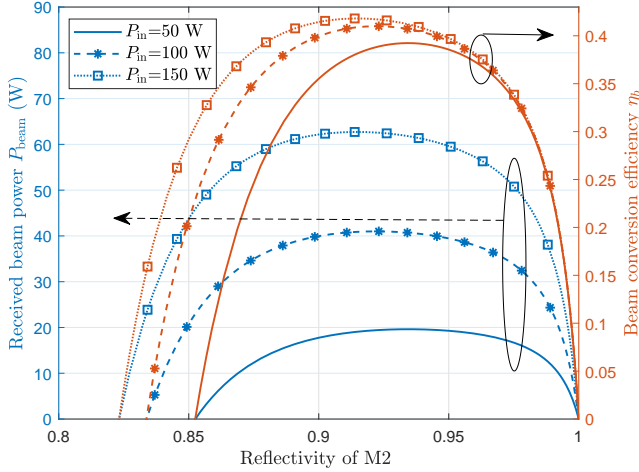


Fig. 9. Received beam power and conversion efficiency versus reflectivity of M2

seen, as l increases, P_{beam} and η_b will also rise. However, the trend of increase tend to be flat when the thickness of the effective gain layer takes a large value. The influence of the l on P_{beam} and η_b become inconspicuous. Moreover, when P_{in} take a large value, curves of P_{beam} and η_b will move up. In numerical, the received beam power can be 60 W and beam conversion efficiency can be 40 % as $P_{\text{in}}=150$ W, the increase of P_{in} has great impact on P_{beam} while has insignificant impact on η_b . Overall, we can improve the performance of beam transmission by raising the thickness properly.

Then, Fig. 9 presents the curves of received beam power and conversion efficiency versus reflectivity of M2. It can be seen from the blue lines, as reflectivity of M2 (R_2) changes from 0.8 to 1, both received beam power and beam conversion efficiency will increase and then decrease. Moreover, when input power enhancing, curves of P_{beam} and η_b will advance to the left and ascending. Numerically, the maximum value of P_{beam} and η_b are obtained when the R_2 locates at the range

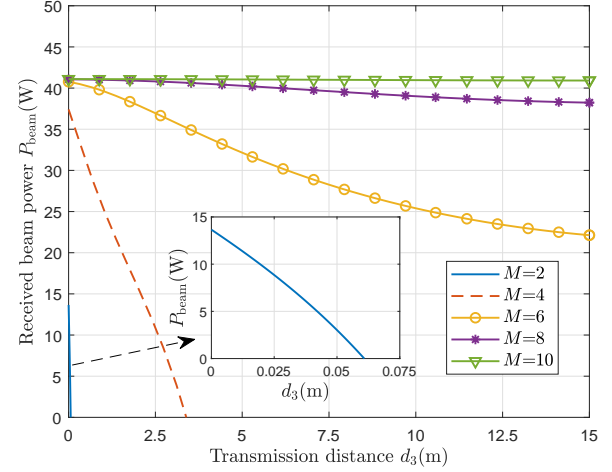


Fig. 11. Received beam power versus transmission distance

from 0.9 to 0.95.

In Fig. 10, we analyze P_{beam} and η_b as the function of the input power P_{in} . According to the blue lines, the P_{beam} will increase as P_{in} increase, which presents a positive linear relationship with P_{in} . Moreover, the slope and intercept of lines are affected by R_2 . A large value of R_2 is benefit for reducing the threshold power (line intercept). Besides, from the red curves, the η_b will be also enhanced by P_{in} increase. However, different from P_{beam} , curves are nonlinear and gradually flattens out. Further, we evaluate the performance of received beam power P_{beam} as the function of transmission distance d_3 , which is shown in Fig. 11. As can be seen, curves of P_{beam} present a downtrend with the increase of the d_3 which proves the negative impact of the transmission loss on beam output (Section II.C). What's more, with the value of M increases, curves become flattened. It indicted that the transmission loss can be restrained by TIM. In numerical, the value of P_{beam} can maintain 40W output over 15m distance.

TABLE II
COMPARISON OF EXISTING SWIPT SCHEMES

Technology	Ref.	Conversion Efficiency	Spectral Efficiency	Output Power	Transmission Distance
Visible light	[41]	$0.38 \times 10^{-4} \%$	6 bit/s/Hz	2.96 mW	1.5 m
	[42]	$8.44 \times 10^{-5} \%$	8 bit/s/Hz	0.38 mW	3.0 m
Radio frequency	[43]	$1.375 \times 10^{-4} \%$	Not stated	$5.5 \mu\text{W}$	15 m
	[44]	$5 \times 10^{-2} \%$	7 bit/s/Hz	5 mW	10 m
Resonant beam	[13]	1%	Not stated	2W	2.6 m
	This work	11%	18 bit/s/Hz	16W	15 m

C. Output Electric Power and Channel Capacity

To evaluate the received beam power, we have analyzed the influence factor of the P_{beam} and η_b . Further, the performance of PV and APD for simultaneous wireless information and power transfer need to be analyzed.

1) *Parameter Setting*: To evaluate the SWIPT performance, we should define the PV and APD parameters at first. According to [34], PV cell structure parameters η_p and P_{pth} are set as 0.3487 and -1.535 W, respectively. In the proposed system, the environment temperature is taken as $T=300$ K, the electronic charge q is 1.6×10^{-19} C, and the Boltzmann constant k is 1.38×10^{-23} J/K. The APD for light signal receiving is commercial sensors for 980 nm wavelength. According to [36], [38]–[40], we set the conversion responsivity of the APD $\nu=0.6$ A/W, the noise bandwidth $B_x=811.7$ MHz, the background current $I_{\text{bg}}=5100$ μA , and the load resistance $R_L=10$ K Ω .

2) *Calculation results and analysis*: Fig 12 depicts curves of spectral efficiency, output electric power, and end-to-end conversion efficiency versus beam splitting ratio. As can be seen from the blue line, entirety curve presents a downward trend with an increase of μ . The decline of the curve is relatively gentle at the beginning. When μ is greater than 0.8, \tilde{C} begins to drop sharply. Then, from the red and green lines with markers, both P_{Eout} and η_E have positive linear relationship with μ . The value of them will increase with μ increase. In numerical, the spectral efficiency \tilde{C} can be 17.69 bit/s/Hz when μ takes 0.99, where P_{Eout} and η_E can also be high. Thus, we can adopt it to be the beam splitting ratio to achieve high-efficiency SWIPT.

Besides, we further explore the relationship of spectral efficiency, output electric power, and end-to-end conversion efficiency versus input power, which is presented in Fig. 13. As can be seen from the blue line, the spectral efficiency will fast rises to a larger value. Overall, the greater the input beam energy, the higher spectral efficiency of the scheme will obtain. However, this influence is relatively limited. With the input power continues to increase, the spectral efficiency of the system will be stable. When P_{in} increases from 50W to 150W, the spectral efficiency only increases 1 bit/s/Hz. Furthermore, according to the red and green lines, both the P_{Eout} and η_E have positive relationship with P_{in} where the P_{Eout} is liner and η_E is nonlinear. Numerically, P_{Eout} and η_E can up to 16 W and 0.11 at $P_{\text{in}} = 150$ W. Generally, through reasonable matching of splitting ratio and input power, the system's data transmission spectral efficiency can reach up to 16-18 bit/s/Hz, and support 0-16 W electric power, which proves that the

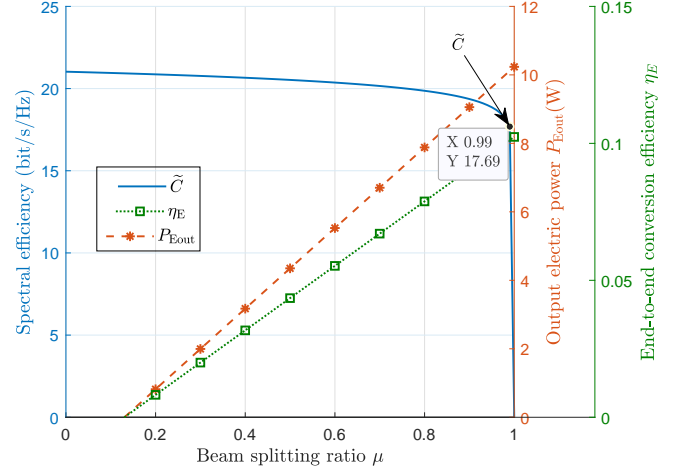


Fig. 12. Spectral efficiency, output electric power, and end-to-end conversion efficiency versus beam split ratio ($P_{\text{in}}=100$ W)

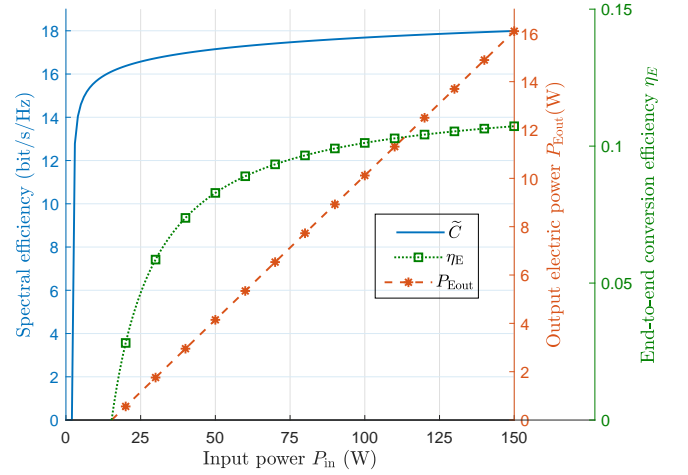


Fig. 13. Spectral efficiency, output electric power, and end-to-end conversion efficiency versus input power ($\mu=0.99$)

system has the potential for high-rate and high-power SWIPT.

D. Summary

In summary, after numerical evaluation and analysis, we can know that the proposed RB SWIPT scheme is capable of providing 16 W electrical energy harvesting and 18 bit/s/Hz spectral efficiency for communication, with 11% energy conversion efficiency and 10 m transmission distance. Table II

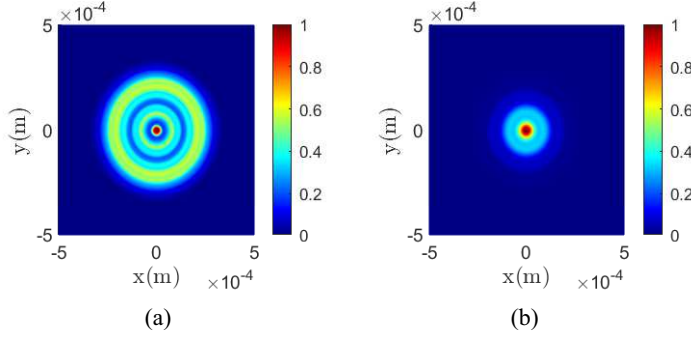


Fig. 14. Field distribution on the gain medium: (a)without TIM; (b)with TIM

presents the performance comparison between our system and the existing architectures. It is clear that the proposed RB SWIPT has benefits in that it can deliver high power while also permitting high spectrum efficiency and energy conversion efficiency over long transmission distance

IV. DISCUSSION

A. Transmission Model by Electromagnetic Field Propagation

In the aforementioned Sections, we have developed end-to-end beam transmission model by beam matrices based on the linear optics. Further, due to the electromagnetic field characteristics of light waves, we can also adopt electromagnetic field propagation to conduct exact analyses for the amplitude and phase distribution of the light field. The description of electromagnetic field propagation is derived by using Maxwell's equations to develop the wave equations for the electric and magnetic fields [45]. Furthermore, according to Huygens-Fresnel principle, during the propagation of light, the field distribution at any point is determined by the coherent superposition of the wavelets of the incident wave at that point [46]. Thus, if we know the field distribution of the initial point light wave $u(x, y)$, according to diffraction theory, its field distribution at point s of the transmission path $u'(x, y)$ can be expressed. Then, we can depict the beam transmission in the resonator. Based on it, we can substitute the resonator boundary conditions of the proposed system and describe the light field change of the beam after an end-to-end cycle. Finally, taking the beam generation from the self-reproductive mode [47] as the judgment condition for stable output, we can obtain the light field distribution at steady state.

Fig. 14 presents the field distribution on the gain medium based on the electromagnetic field propagation model. As can be seen, the incident beam on the gain medium has been effectively compressed in the proposed system with TIM. In contrast, beam has a large field distribution with low beam quality (uneven distribution) in the original system without TIM. Aforementioned analysis correspond to the results obtained by using the matrix model in section V, which further verifies the feasibility of the proposed scheme. Overall, the electromagnetic field propagation can be used to analyze the field distribution of the beam, which is benefit to evaluate the beam's quality, system structure, etc. However, it is worth noting that in the process of changing the calculation, the fast

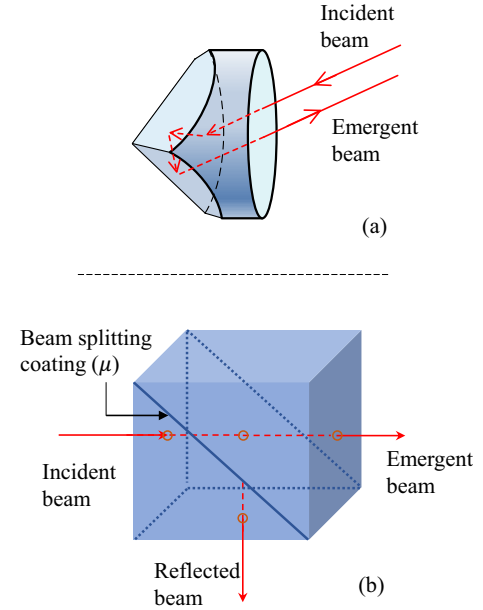


Fig. 15. (a) Corner-cube reflector; (b) Cube beam-splitter

Fourier transform and the Fox-Li iterative method are adopted in the calculation, but compared with the transmission matrix proposed in the second section of this paper, its computing power requirements and time consumption are still too large. In future research, we will explore in more depth the results and advantages of using this method.

B. System Experiment and Applications

In this paper, we propose a scheme for high-efficiency RB charging and communication, provide the analytical model, and evaluate the system performance by simulation. Further, to adopt proposed RB-SWIPT scheme in IoT applications, we will herein discuss the experimental deployment of the system.

1) System structure: As it shows in Fig. 2 and 5, several lenses are involved in the system. Their materials can be N-BK7 glass with high laser damage threshold, and their surface should cover with anti-reflective coating for reducing beam loss. Reflectors M1 and M2 can be designed as cat-eye structure which is depicted in Section II.C. They comprise a convex lens and a flat mirror arranged in parallel, with their pupils overlapping to form a focus-free system. Moreover, reflectors with corner-cube structure (Fig. 15.(a)) can also be applied in this system for beam retro-reflecting. To realize beam separated, optical splitters are introduced in the receiver. Normally, beam splitters such as cube beam-splitters can be used to separate the external beam, which are demonstrated in Fig. 15(b). Cube beam-splitter consists of two classical right angle prisms which can also consist by N-BK7 glasses. The hypotenuse surface of one prism has a coating for beam splitting, and the two prisms are cemented together, forming a cubic shape. When beams incident, part of the beam will transmit through it, and the other part of the beam is reflected by the coating and propagates in the vertical incident direction.

As the gain module we employ is an open-cavity surface-emitting semiconductor gain, customization is necessary. As illustrated in Fig. 2, the entire semiconductor gain module consists of multiple power supply modules from different regions. Among these, the middle Distributed Bragg Reflector (DBR) layer and the gain layer are generated by material growth equipment, including the multi-layer stack structure of high and low refractive indices and the quantum well structure mentioned earlier. The top layer is the photon exit for light emission, onto which an antireflection coating structure can be deposited to reduce optical loss. The bottom layer is a thermal layer for heat dissipation, which can be a high thermal conductivity metal compatible with semiconductor materials. In addition, at the receiving end, we can use a programmable power supply to change the input state of the pump source by way of amplitude modulation, thus loading the data into the system. Based on the analysis of the aforementioned experimental key points, combined with a rational deployment of components, the experimental platform can be constructed.

2) System applications: In order to illustrate the practicality of our system, we will provide an example of its application in real-time IoT scenarios. The exceptional mobility of unmanned aerial vehicles (UAVs) makes them ideal candidates for serving as air nodes, enabling the extension of network coverage and enhancing the flexibility of the IoT topology. However, this imposes higher requirements on the system's endurance and communication capabilities. To effectively power UAVs and supply dependable data transmission, the RB-SWIPT system can be utilized. Specifically, we can design a compound UAV system, which consists of a short-endurance UAV, a RB-SWIPT station, and a group of buoy sensors. The receiver module of the RB-SWIPT station is implanted in the fuselage of the UAV, enabling it to be wirelessly charged through resonant beam technology. Additionally, when the UAV needs to collect sensing data reliably from the sensors and adjust its flight path or act as a "thing" node in the IoT network, resonant beam can effectively transmit the data. This allows for a higher state of charge (SOC) of the UAVs to be achieved. In the original resonant optical system, the transmission distance and conversion efficiency are limited due to energy loss, with a transmission distance of only 2.6 meters and a conversion efficiency of just 1% [13]. This made it difficult for the system to be applied in UAVs. However, the new scheme proposed in this paper, based on a telescope structure and high-efficiency semiconductor gain modules, significantly improves the transmission distance and conversion efficiency, making it possible for the resonant optical system to be applied in UAVs. Moreover, we have designed a viable communication path that allows for energy transmission and information delivery to occur simultaneously. The reliable optical communication channel solves issues related to bandwidth and interference, making UAVs effectively function as nodes in Internet of Things (IoT) applications. In addition to the UAV case cited above, a variety of real-time IoT terminals can also be integrated with RB-SWIPT systems. For example, human body sensors, cameras, smart doorbells, etc. By implementing the proposed system, issues such as device wiring, excessive

battery usage, and radio signal interference can be effectively mitigated through real-time energy and signal transmission.

V. CONCLUSIONS

In this paper, we proposed a high-efficiency resonant beam charging and communication system using the semiconductor gain medium and the telescope internal modulator. Relying on theories of beam transmission, power conversion, energy harvesting, and data receiving, we have established analytical models for the beam propagation, beam power, electric power output, and spectral efficiency of the proposed system. Numerical results illustrate that the system present a remarkable SWIPT performance. Compared with the original system, it can achieve efficient beam compression, the high power output, energy conversion efficiency enhanced, and high spectral efficiency for high-efficiency resonant beam charging and communication.

There are compelling topics that warrant further investigation in future studies. 1) With respect to the performance of the proposed scheme during actual deployment, its influencing factors, and the discrepancies with the simulation results, the experimental analysis of the system can be conducted in the future. 2) The integration of the proposed system scheme into existing IoT devices, such as system integration, energy reception circuit design, and communication module design, should be thoroughly researched in the future.

REFERENCES

- [1] M. Series, "IMT vision—framework and overall objectives of the future development of IMT for 2020 and beyond," *Recommendation ITU*, vol. 2083, 2015.
- [2] K. Jin and W. Zhou, "Wireless laser power transmission: a review of recent progress," *IEEE transactions on power electronics*, vol. 34, no. 4, pp. 3842–3859, Jul. 2018.
- [3] S. Y. R. Hui, W. Zhong, and C. K. Lee, "A critical review of recent progress in mid-range wireless power transfer," *IEEE Transactions on Power Electronics*, vol. 29, no. 9, pp. 4500–4511, Mar. 2013.
- [4] X. Lu, P. Wang, D. Niyato, D. I. Kim, and Z. Han, "Wireless charging technologies: Fundamentals, standards, and network applications," *IEEE Communications Surveys & Tutorials*, vol. 18, no. 2, pp. 1413–1452, Nov. 2015.
- [5] J. Lim, T. S. Khwaja, and J. Ha, "Wireless optical power transfer system by spatial wavelength division and distributed laser cavity resonance," *Opt. Express*, vol. 27, no. 12, pp. A924–A935, Jun 2019.
- [6] Y. Huang and B. Clerckx, "Waveform design for wireless power transfer with limited feedback," *IEEE Transactions on Wireless Communications*, vol. 17, no. 1, pp. 415–429, Nov. 2017.
- [7] B. Scrosati and J. Garche, "Lithium batteries: Status, prospects and future," *Journal of power sources*, vol. 195, no. 9, pp. 2419–2430, May. 2010.
- [8] R. W. Habash, J. M. Elwood, D. Krewski, W. G. Lotz, J. P. McNamee, and F. S. Prato, "Recent advances in research on radiofrequency fields and health: 2004–2007," *Journal of Toxicology and Environmental Health, Part B*, vol. 12, no. 4, pp. 250–288, Aug. 2009.
- [9] H. Elgala, R. Mesleh, and H. Haas, "Indoor optical wireless communication: potential and state-of-the-art," *IEEE Communications Magazine*, vol. 49, no. 9, pp. 56–62, Sept. 2011.
- [10] H. Li and Y. Huang, "The architecture of blind equalizer for mimo free space optical communication system," in *Optical Communication, Optical Fiber Sensors, and Optical Memories for Big Data Storage*, vol. 10158. International Society for Optics and Photonics, Oct. 2016, p. 101581H.
- [11] A. Ortal, Z. Nes, P. Rudiger, and Zurich, "Wireless laser system for power transmission utilizing a gain medium between retroreflectors," U.S. Patent 9 653 949, May 16, 2017.

- [12] Q. Liu, J. Wu, P. Xia, S. Zhao, W. Chen, Y. Yang, and L. Hanzo, "Charging unplugged: Will distributed laser charging for mobile wireless power transfer work?" *IEEE Vehicular Technology Magazine*, vol. 11, no. 4, pp. 36–45, Dec. 2016.
- [13] W. Wang, Q. Zhang, H. Lin, M. Liu, X. Liang, and Q. Liu, "Wireless energy transmission channel modeling in resonant beam charging for IoT devices," *IEEE Internet of Things Journal*, vol. 6, no. 2, pp. 3976–3986, Apr. 2019.
- [14] M. Liu, H. Deng, Q. Liu, J. Zhou, M. Xiong, L. Yang, and G. B. Giannakis, "Simultaneous mobile information and power transfer by resonant beam," *IEEE Transactions on Signal Processing*, pp. 1–1, May. 2021.
- [15] W. Fang, H. Deng, Q. Liu, M. Liu, Q. Jiang, L. Yang, and G. B. Giannakis, "Safety analysis of long-range and high-power wireless power transfer using resonant beam," *IEEE Transactions on Signal Processing*, May. 2021.
- [16] M. A. Khalighi and M. Uysal, "Survey on free space optical communication: A communication theory perspective," *IEEE communications surveys & tutorials*, vol. 16, no. 4, pp. 2231–2258, Jun. 2014.
- [17] W. Chen, S. Zhao, Q. Shi, and R. Zhang, "Resonant beam charging-powered UAV-assisted sensing data collection," *IEEE Transactions on Vehicular Technology*, vol. 69, no. 1, pp. 1086–1090, Oct. 2019.
- [18] X. Liu, Y. Liu, Y. Chen, and L. Hanzo, "Trajectory design and power control for multi-UAV assisted wireless networks: A machine learning approach," *IEEE Transactions on Vehicular Technology*, vol. 68, no. 8, pp. 7957–7969, May. 2019.
- [19] Q. Sheng, M. Wang, H. Ma, Y. Qi, J. Liu, D. Xu, W. Shi, and J. Yao, "Continuous-wave long-distributed-cavity laser using cat-eye retroreflectors," *Opt. Express*, vol. 29, no. 21, pp. 34 269–34 277, Oct. 2021.
- [20] Z. Zhang, J. Zhang, Y. Zhou, X. Zhang, Z. Li, J. Zhang, J. Zhang, Y. Gong, T. Liu, J. Mu *et al.*, "2m-distance external cavity vecsel for wireless charging applications," *Optics Express*, vol. 30, no. 13, pp. 22 364–22 375, Jun. 2022.
- [21] M. Xiong, M. Liu, Q. Zhang, Q. Liu, J. Wu, and P. Xia, "TDMA in adaptive resonant beam charging for IoT devices," *IEEE Internet of Things Journal*, vol. 6, no. 1, pp. 867–877, Feb. 2018.
- [22] M. Xiong, Q. Liu, M. Liu, X. Wang, and H. Deng, "Resonant beam communications with photovoltaic receiver for optical data and power transfer," *IEEE Transactions on Communications*, vol. 68, no. 5, pp. 3033–3041, Feb. 2020.
- [23] M. S. Aziz, S. Ahmad, I. Husnain, A. Hassan, and U. Saleem, "Simulation and experimental investigation of the characteristics of a pv-harvester under different conditions," in *2014 International Conference on Energy Systems and Policies (ICESP)*. IEEE, Nov. 2014, pp. 1–8.
- [24] J. C. Campbell, "Recent advances in telecommunications avalanche photodiodes," *Journal of Lightwave Technology*, vol. 25, no. 1, pp. 109–121, Jan 2007.
- [25] W. W. Chow, S. W. Koch, and M. I. Sargent, *Semiconductor-laser physics*. Springer Science & Business Media, 2012.
- [26] H. Soda, K. ichi Iga, C. Kitahara, and Y. Suematsu, "GaInAsP/InP surface emitting injection lasers," *Japanese Journal of Applied Physics*, vol. 18, no. 12, pp. 2329–2330, dec 1979.
- [27] H. Soda, Y. Motegi, and K. Iga, "GaInAsP/InP surface emitting injection lasers with short cavity length," *IEEE Journal of Quantum Electronics*, vol. 19, no. 6, pp. 1035–1041, Jun. 1983.
- [28] W. Koechner, *Solid-state laser engineering*. Springer, 2013, vol. 1.
- [29] M. Kuznetsov, F. Hakimi, R. Sprague, and A. Mooradian, "Design and characteristics of high-power (0.5-W CW) diode-pumped vertical-external-cavity surface-emitting semiconductor lasers with circular TEM₀₀ beams," *IEEE Journal of Selected Topics in Quantum Electronics*, vol. 5, no. 3, pp. 561–573, May. 1999.
- [30] P. Baues, "Huygens' principle in inhomogeneous, isotropic media and a general integral equation applicable to optical resonators," *Optoelectronics*, vol. 1, no. 1, pp. 37–44, Feb. 1969.
- [31] V. Magni, "Multielement stable resonators containing a variable lens," *JOSA A*, vol. 4, no. 10, pp. 1962–1969, Oct 1987.
- [32] S. Cao, S. Tu, Y. Huang, H. Fan, J. Li, H. Xia, and G. Ren, "Analysis of diffraction loss in laser resonator," *Laser Technol.*, vol. 42, no. 3, pp. 400–403, May. 2018.
- [33] Q. Zhang, W. Fang, M. Xiong, Q. Liu, J. Wu, and P. Xia, "Adaptive resonant beam charging for intelligent wireless power transfer," *IEEE Internet of Things Journal*, vol. 6, no. 1, pp. 1160–1172, Feb. 2018.
- [34] Q. Zhang, W. Fang, Q. Liu, J. Wu, P. Xia, and L. Yang, "Distributed laser charging: A wireless power transfer approach," *IEEE Internet of Things Journal*, vol. 5, no. 5, pp. 3853–3864, Oct. 2018.
- [35] E. Boshkovska, D. W. K. Ng, N. Zlatanov, and R. Schober, "Practical non-linear energy harvesting model and resource allocation for swipt systems," *IEEE Communications Letters*, vol. 19, no. 12, pp. 2082–2085, Dec. 2015.
- [36] F. Xu, M. Khalighi, and S. Bourennane, "Impact of different noise sources on the performance of PIN- and APD-based FSO receivers," in *Proceedings of the 11th International Conference on Telecommunications*, Jun. 2011, pp. 211–218.
- [37] A. Lapidoth, S. M. Moser, and M. A. Wigger, "On the capacity of free-space optical intensity channels," *IEEE Transactions on Information Theory*, vol. 55, no. 10, pp. 4449–4461, Oct. 2009.
- [38] M. S. Demir, F. Miramirkhani, and M. Uysal, "Handover in VLC networks with coordinated multipoint transmission," in *2017 IEEE International Black Sea Conference on Communications and Networking (BlackSeaCom)*, Jun. 2017, pp. 1–5.
- [39] C. Quintana, Q. Wang, D. Jakonis, X. Piao, G. Erry, D. Platt, Y. Thueux, A. Gomez, G. Faulkner, H. Chun, M. Salter, and D. O'Brien, "High speed electro-absorption modulator for long range retroreflective free space optics," *IEEE Photonics Technology Letters*, vol. 29, no. 9, pp. 707–710, Mar. 2017.
- [40] A. J. Moreira, R. T. Valadas, and A. de Oliveira Duarte, "Optical interference produced by artificial light," *Wireless Networks*, vol. 3, no. 2, pp. 131–140, May. 1997.
- [41] S. Ma, F. Zhang, H. Li, F. Zhou, Y. Wang, and S. Li, "Simultaneous lightweight information and power transfer in visible light communication systems," *IEEE Transactions on Wireless Communications*, vol. 18, no. 12, pp. 5818–5830, Dec. 2019.
- [42] A. M. Abdelhady, O. Amin, B. Shihada, and M.-S. Alouini, "Spectral efficiency and energy harvesting in multi-cell slipt systems," *IEEE Transactions on Wireless Communications*, vol. 19, no. 5, pp. 3304–3318, Feb. 2020.
- [43] X. Lu, P. Wang, D. Niyato, and E. Hossain, "Dynamic spectrum access in cognitive radio networks with rf energy harvesting," *IEEE Wireless Communications*, vol. 21, no. 3, pp. 102–110, Jun. 2014.
- [44] I. Krikidis, S. Timotheou, S. Nikolaou, G. Zheng, D. W. K. Ng, and R. Schober, "Simultaneous wireless information and power transfer in modern communication systems," *IEEE Communications Magazine*, vol. 52, no. 11, pp. 104–110, Nov. 2014.
- [45] R. N. N. Hodgson and I. H. Weber, *Laser Resonators and Beam Propagation*. Springer, 2005, vol. 108.
- [46] T. Teperik, A. Archambault, F. Marquier, and J.-J. Greffet, "Huygens-fresnel principle for surface plasmons," *Optics express*, vol. 17, no. 20, pp. 17 483–17 490, Sept. 2009.
- [47] A. G. Fox and T. Li, "Resonant modes in a maser interferometer," *Bell System Technical Journal*, vol. 40, no. 2, pp. 453–488, Mar. 1961.